Design of industrially scalable microtubular solid oxide fuel cells based on an extruded support

H. Monzón[1], M. A. Laguna-Bercero[1], A. Larrea[1], B.I. Arias[2], A. Várez[2] and B. Levenfeld[2]

[1] *Instituto de Ciencia de Materiales de Aragón (ICMA), CSIC- Universidad de Zaragoza,*

C/ María de Luna 3, E-50018 Zaragoza, Spain

[2]*Dpto. Ciencia e Ingeniería de Materiales. Universidad Carlos III de Madrid.*

Avda. Universidad 30 28911 Leganés, Spain

Corresponding author information:

Miguel A. Laguna-Bercero

malaguna@unizar.es

C/ María de Luna 3, E-50018 Zaragoza, Spain

Phone: +34 876 555152

Fax: +34 976 761957

Abstract

The current work describes the adaptation of an existing lab-scale cell production method for an anode supported microtubular solid oxide fuel cell to an industrially ready and easily scalable method using extruded supports. For this purpose, Ni-YSZ (yttria stabilized-zirconia) anode is firstly manufactured by Powder Extrusion Moulding (PEM). Feedstock composition, extruding parameters and binder removal procedure are adapted to obtain the tubular supports. The final conditions for this process were: feedstock solid load of 65 vol%; a combination of solvent debinding in heptane and thermal debinding at 600 °C. Subsequently, the YSZ electrolyte layer is deposited by dip coating and the sintering parameters are optimized to achieve a dense layer at 1500 ^{0}C during 2 hours. For the cathode, a LSM (lanthanum strontium manganite)-YSZ layer with an active area of ~1 cm^2 is deposited by dip coating. Finally, the electrochemical performance of the cell is measured using pure humidified hydrogen as fuel. The measured power density of the cell at 0.5V was 0.7Wcm^{-2} at 850^{0}C.

Keywords: SOFC, Powder Extrusion Moulding, Microtubular, NiO, YSZ

1- Introduction

Fuel cells represent an efficient and clean way of transforming fuel into electric energy [1-3]. By avoiding the chemical-to-heat and heat-to-mechanical energy transformation steps, a high electric energy yield can be achieved. Solid oxide fuel cells (SOFC) are a type of fuel cell in which the electrolyte is an ion conducting ceramic oxide, commonly, yttria stabilized zirconia (YSZ). This material typically reaches an acceptable value of ionic conductivity at working temperatures between 600 and 1000^{0}C, being 800^{0}C probably the most extended working temperature. These high operation temperatures grant fuel molecules enough energy for dissociation to occur in presence of low activity catalysts such as nickel, while lower temperature fuel cells generally need higher catalytic power, usually found in precious metals. Moreover, high temperature operation allows fuel reforming and thus enabling the use of hydrocarbon-based fuels. Fuel reforming can be external, taking advantage of the wasted heat, or internal on nickel in the anode.

Among the different configurations of SOFCs (planar, conventional tubular and micro- tubular), the microtubular configuration overcomes the drawback of the excessive heating and cooling time of the conventional solid oxide cells. The use of small (less than 4 mm) tubes as ceramic support enhances the mechanical strength and thermal shock resistance of the cell [4]. As a consequence, microtubular SOFCs are an excellent candidates for portable applications[5], and their development is only slightly behind the comparable SOFC status [6]. In addition microtubular SOFC can also be used for high temperature steam electrolysis [7, 8].

Electrode composition and microstructure play a major role in SOFC electrochemical performance, and those parameters are usually conditioned or limited by the processing path. For this reason, fabrication methods are a major topic in microtubular SOFC research. These methods include cold isostatic pressing [9, 10], slip casting [11], extrusion [12-14], gel casting

[15], electro-phoretic deposition [16] and phase inversion co-extrusion [17] amongst others. Some features are desired on every production method such as reproducibility, geometrical quality and scalability amongst others. These standards are frequently not met by lab-scale methods and, in some cases, the lack of them can become performance limiting in the resultant cell. Among the aforementioned methods, extrusion is the most promising one for massive substrate production because of its low-cost and well-established technologies. The problems associated with extrusion are mainly related to the binder removal and firing processes. They include lack of straightness, defects in the walls, eccentric shapes, warped and twisted tubes as well as bubble formation [6]. It is also worth mentioning that there is a lack of information in the scientific literature regarding the technical details on the extrusion procedure for microtubular SOFCs.

The current work describes the adaptation of an existing lab-scale cell production method [18] to an industrially ready and easily scalable method using extruded supports. Anode support optimization was carried out via cold isostatic pressing (CIP) on previous works [4, 8, 19]. Based on these previous studies, the selected final composition for the anode support is: 50% porosity, 25% nickel and 25% YSZ in volume. In the present work, the use of corn starch as pore former is reported in a ceramic powder extrusion process for the first time, producing spherical pores (diameter about 10 μm). The whole cell fabrication route selected on this study consists of an extruded anode support, whereas both electrolyte and cathode are deposited by dip coating. The new process has numerous advantages such as an increase in the production capacity, in reproducibility and also in the mechanical properties of the green body, which facilitates handling and later processing steps.

2- Materials and methods

2.1- Anode compounding and extrusion

For the extrusion process, a powder formulation based on NiO (Hart Materials), YSZ (Tosoh) and corn starch as pore-former in a composition based on previous studies [4]. Final composition of the anode support is Ni–YSZ ratio of 50:50 (% in volume of solid phase), with porosities near 50%.The binder system consists of polypropylene (supplied by Repsol YPF), paraffin wax (Panreac) and stearic acid (Panreac). A similar binder system was previously used for manufacturing of YSZ thin tubes [20]. Four powder mixtures were formulated containing 45, 55, 60 and 65 vol% solid loading. Firstly, different feedstock formulations were compounded in a Haake Rheocord 252 mixer with a pair of roller rotor blades at 170^{o}C and 40 rpm. During the mixing process, the torque values were recorded. In order to determine the optimal feedstock formulation, the rheological characterization was performed in a ThermoHaake capilar rheometer at 170^{0}C covering a shear rate from 100 to 10000s^{-1}.

Subsequently, the tubes were extruded using a single screw extruder (Haake Polylab) with a home-designed extrusion die connected to the extruder [20]. Screw speed and temperature profile were tuned in order to obtain an extruded body able to sustain its own weight as well as to avoid deformation before cooling. Extrusion was made vertically into a water bath to reduce the solidification time. A combination of solvent and thermal debinding process was carried out to remove the organic part. Solvent debinding step was then applied to the samples consisting on an n-heptane bath at 60^{0}C overnight. Thermogravimetric analysis (TGA) was performed under air atmosphere using a Perkin Elmer TGA1 thermogravimetric analyzer. Thermal debinding cycle consisted on a heating ramp at 1°Cmin^{-1} up to 600^{o}C.

2.2- Electrolyte deposition

A dilatometry test was run on a solvent debound sample in order to determine its sintering behaviour using a thermo-mechanical analyzer (Setaram, SETSYS 200, France). The same test was run on TZ-8Y and TZ-8YS powders (Tosoh), to be used as the solid electrolyte. Both powders are 8 mol% Y_2O_3 in ZrO_2 (99.9%), presenting average crystallite sizes of 23 and 52 nm respectively.

A suspension was prepared with TZ-8YS powders in an isopropanol –ethanol azeotropic mixture, using PVB (polyvinyl butyral) as binder and Beycostat as dispersant agent. Solvent debound anode support samples were cut into 6.75 cm (in length) samples and dipped 3 times at a drawing rate of 3 mm s^{-1}. A 5 mm long section was left uncovered on each side of the support to facilitate the later anode electrical contact and sealing. Samples were then sintered at different temperatures (from 1350 to 1600^{0}C) in order adjust the sintering conditions.

2.3- Cathode deposition

After adjusting the sintering conditions for anode-electrolyte half cells, the LSM-YSZ cathodes were deposited. For this purpose, two cathode suspensions were prepared, the first one using a 1:1 (vol%) ratio of LSM (Fuel cell materials) and TZ-8YS (Tosoh), acting as the functional layer, and a second one using a 4:1 ratio of the same materials to enhance current collection. For both suspensions, the dispersing medium and additives were identical to that of the electrolyte suspension. An active area of ~1 cm^2 of cathode was deposited on each cell, consisting of 2 dips of the 1:1 suspension and 2 dips of the 4:1 suspension, at a 3 mms^{-1} drawing rate. Once cathode had been deposited, the cells were sintered at 1150^{o}C for 90 min. Final dimensions of the cells are 50 mm in length; wall thickness of about 700 µm; outer diameter of 3.4 mm; electrolyte thickness of 22 µm; and total cathode thickness of about 34 µm.

2.4- Electrochemical and microstructural characterization

Electrical contacts were made using platinum wire in a four probe setup. Anode contacts were made through the uncovered edges, in a similar manner to that described by Suzuki et al. [21]. Due to the good connectivity of Ni particles at the anode support, no current collection losses were detected with this method, in comparison with our previous manner when using Ni mesh inside of the tube [4,6]. Cathode current collection was made by coiling the wire around the deposited section and adding small amounts of Pt paste to improve electrical contact. We have confirmed that there is no enhancement in fuel cell performance due to Pt catalysing oxygen reduction reaction, as similar results were obtained when using gold as current collectors. This effect is consistent with the fact that the outer cathode layer contains a non-percolating ionic conductor phase (only 20% in volume of YSZ, as observed in fig. 5), so that oxygen reduced on the metal contact has no ionic path to the electrolyte. We have also observed that almost no lateral conduction losses were detected at the cathode, as the ohmic resistance measured by EIS (electrochemical impedance spectroscopy) is very close to the resultant according with the conductivity of the YSZ electrolyte. The cells were then sealed to alumina tubes using refractory clay and placed inside a home-made small tubular furnace. Nitrogen was fed into the anode side of the cell during the heating process at a heating rate of $20^{0}Cmin^{-1}$. After stabilization of the temperature at $800^{0}C$, pure humidified hydrogen was fed to the cell, reducing NiO to metallic Ni at the anode whereas the cathode side was left to ambient air. j-V (current density-voltage) and EIS measurements were performed using a VSP Potentiostat/Galvanostat (Princeton Applied Research, Oak Ridge, US).

Microstructural characterization of polished cross-section samples was performed using a field emission scanning electron microscope (Merlin FE-SEM, Carl Zeiss).

3. Results and discussion

3.1- Powder extrusion moulding of NiO-YSZ microtubes

As the final ceramic microstructure and composition had been optimized in a previous work, we have prepared various feedstocks with different solid powder loading (45, 55, 60 and 65 vol. %) using the same powder formulation. Considering that the powder contains pore former, and NiO reduction increases the porosity of the compact, we have optimized the feedstock on the basis of a maximum solid loading with appropriated rheological characteristics. This is performed in order to minimize problems associated with binder removal and shrinkage during densification and also to obtain defect-free shapes. Torque measurements showed that all the prepared feedstock presented good homogeneity, appropriate torque values and thermoplastic behaviour (Fig. 1), which is the most suitable for extrusion process. As expected, the viscosity increases with powder loading. The reached values were less than 1000 Pa s, which is the desirable limit for an adequate extrusion process. Therefore, feedstock with 65 vol. % of powder loading was finally chosen.

The dimensions of the extruded green tubes were 4 mm outer diameter, around 1 mm wall thickness and 12 cm in length. The extrusion parameters were optimized in order to obtain a homogeneous extrusion profile.

After the extrusion process, elimination of polymeric part was carried out. As a first approach, a conventional thermal debinding was tested. However, blistering occurred in all the samples, even when using a very low heating rate, being this a consequence of the violent removal of the most volatile components of the binder system (paraffin wax and stearic acid). In order to prevent the presence of these defects, a combination of solvent and thermal debinding was carried out. After soluble binder removal, an interconnected pore channel is formed from exterior to interior of the tubes, which serves as escape path for decomposed gas during subsequent thermal debinding of insoluble binder components.

TGA experiments (figure 2) performed for a solvent debound sample showed two decomposition steps corresponding to the elimination of polypropylene (at ~180^{o}C), and corn starch (~240^{o}C). This result confirmed that most of the stearic acid and paraffin wax had been previously removed during the solvent debinding step. TGA experiment also showed that organic removal takes place up to approximately 500^{o}C. Consequently, the thermal cycle was programmed at 600^{o}C for 1h to assure a complete removal of the organic components. Similarly, a heating rate of 1^{o}C/min was used in order to prevent surface cracks and internal bubbles.

3.2- Anode-electrolyte cosintering

Dilatometric studies were performed for YSZ powders presenting crystallite sizes of 23 and 52 nm and for the supporting NiO/YSZ tubes in order to achieve a homogeneous shrinkage between the anode and the electrolyte. Attending to the contraction curves, (figure 3), the coarser YSZ powder was selected; as it matches better with the anode support contraction curve. After selecting the appropriate YSZ powder, different anode-electrolyte cosintering temperatures were tested. Samples sintered at 1350 and 1400^{o}C showed cracking and pinholes respectively, displaying a contraction mismatch between support and thin electrolyte. Samples sintered at 1450 and 1500^{o}C presented a smooth uniform appearance. Sample sintered at 1600^{o}C showed a perfectly smooth and transparent electrolyte, but the cell was bent during sintering and the used crucible showed massive contamination after the process, evidencing a material loss (NiO evaporation) and possible microstructure degradation. As a consequence, samples sintered at 1450 and 1500^{o}C were finally selected for further characterization. Figure 4 showed that both samples presented some amount of closed porosity, being the overall amount of porosity observed greater for the sample sintered at 1450^{o}C. Both samples showed electrolyte thickness around 22 µm. After anode and electrolyte

cosintering cathode deposition was performed by dip coating and sintered as described in section 2.3. Figure 5 shows a detail of the microstructure of the cell.

3.3- Electrochemical performance

The j-V curves of the cells sintered at 1450 and 1500 °C were measured at 800 and 850^{o}C (figure 6). Sample sintered at 1450^{o}C is clearly outperformed by the cell sintered at 1500^{o}C, power density values at 0.5V and 850^{o}C are 0.35 and 0.7 Wcm^{-2}, respectively. A comparison of fuel cell performance for the cell sintered at 1500^{o}C and a cell fabricated by cold isostatic pressing of identical composition is shown in figure 7 [4]. In this figure it is possible to observe a slight enhancement in terms of performance. This power density is comparable to state of the art extruded microtubular cells based on similar materials. Dikwal et al performed degradation tests on AMI extruded commercial cells starting from a maximum power output of 0.6 Wcm^{-2} at 800^{o}C [12]. Lee et al assembled a 700 W stack from extruded cells and introduced a design improvement to rise their power output from 0.24 to 0.54 Wcm^{-2} at 0.7V [14].

The recorded EIS spectra (figures 8a and 8b)were measured under open circuit voltage conditions and have been fitted to an equivalent circuit model using the least squares method. There is no agreement in the literature about how the different processes effectively contribute to the impedance of each electrode. For the LSM-YSZ electrode, up to 5 processes have been proposed as contributing [22-24], and a similar number is proposed for the Ni-YSZ electrode [25]. Based on the previous literature, the model proposed in this work (as shown in figure 9) contemplates 5 different major contributions to the whole cell impedance, consisting of an ohmic resistance (R_e), a condenser-resistance element in parallel (R_1C_1), a resistance-constant phase element in parallel (R_2CPE_2), and two finite length Warburg elements (W_3 and W_4). These elements account respectively for the electrolyte and lateral conduction through electrodes, cathode charge transfer, anode charge transfer and gas diffusion through anode and cathode. The use of this model has been also validated for measurements performed

under current load. However, the assignation of the different processes is still tentative as a full analysis under different DC current bias and partial pressures at both anode and cathode is currently being performed. As expected, the cell sintered at 1500^{o}C showed better ASR values, probably resulting from a more densified microstructure. EIS measurements reveal a larger ohmic resistance for the sample sintered at 1450^{o}C, as a consequence of poor electrolyte sintering. Those results are consistent with SEM micrographs (figure 4), that revealed a higher extent of densification and grain growth for the sample sintered at 1500^{o}C. Cathode charge transfer resistance appeared to be identical for both samples whereas cathode diffusion resistance appeared lower for the sample sintered at 1500^{o}C, although no difference was noticed during post mortem examination on the cathode side. Anode charge transfer resistance was found lower in the sample sintered at 1500^{o}C.

4- Conclusions

Powder extrusion moulding was presented in this work as an advantageous technology to obtain a Ni-YSZ porous anode support. The production method adaptation was successful, resulting in a less time consuming fabrication process, which can be easily scaled up to an industrial production level. The final conditions for this process were: feedstock solid load of 65 vol%; a combination of solvent debinding in heptane and thermal debinding at 600 °C. In order to achieve an optimum match between the contraction of anode support and the electrolyte, coarse YSZ was deposited and sintered at 1500 °C during 2 hours. Handling of the green bodies has also been significantly improved in comparison with the CIP method. Additionally geometrical quality has been significantly improved, increasing reproducibility. At 850^{0}C, the power density at 0.5V was 0.7Wcm^{-2} and ASR at OCV was 0.9 Ωcm^{2}. The obtained values are similar to state of the art YSZ based SOFC.

5 – Acknowledgements

Authors would like to thank financial support received from MICINN and Feder program of the European Community (MAT2012- 30763 and MAT2010-19837-CO6 projects), Madrid regional government (MATERYENER S2009 PPQ-1626 program), and also grant GA-LC-035/2012, financed by the Aragón Government and La Caixa Foundation.

Figure captions

Fig. 1. Viscosity measurements for the 45 (solid squares), 55 (hollow squares), 60 (solid circles) and 65 (hollow circles) solid vol% feedstocks. Sample containing a 65 solid mass% could not be measured on the whole range due to instrument limitations.

Fig. 2. TGA experiment for extruded material after solvent debinding.

Fig. 3. Contraction curves for extruded material (solid line) and the proposed electrolyte materials: TZ-8Y (dotted line) and TZ-8YS (dashed line).

Fig. 4. SEM images showing an electrolyte detail for samples sintered at 1500^{o}C (a) and 1450^{o}C (b).

Fig. 5**.** SEM image showing a detail of the microstructure of the cell.

Fig. 6. j-V measurements for the samples sintered at 1500^{o}C (a) and 1450^{o}C (b) at temperatures of 850^{o}C (black) and 800^{o}C (grey)

Fig. 7. j-V measurements at 850^{o}C comparing a CIP supported and an extruded supported samples.

Fig.8. EIS measurements at 850^{o}C for the extruded samples sintered at 1500^{o}C (a) and 1450^{o}C (b).

Figure 1

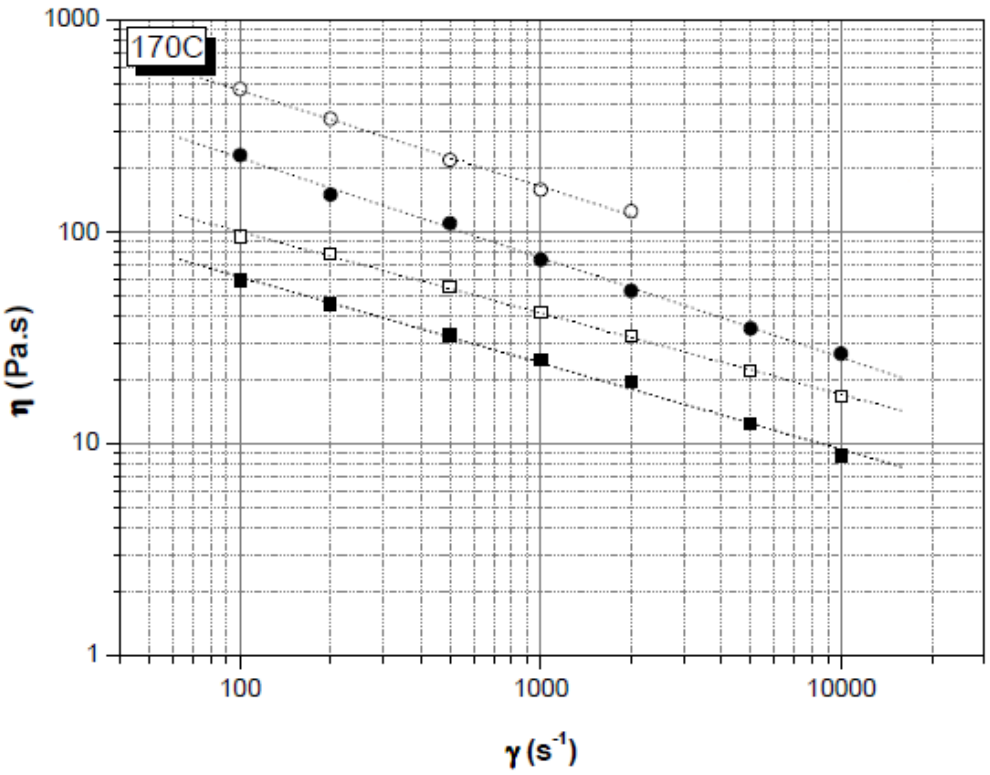

Figure 2

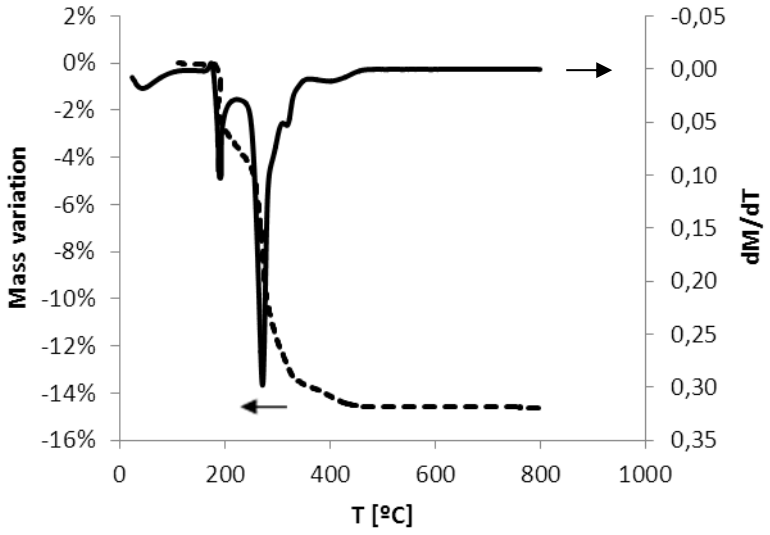
2%
0%
-2%
-4%
-6%
-8%
-10%
-12%
-14%
-16%
Mass variation
-0,05
0,00
0,05
0,10
0,15
0,20
0,25
0,30
0,35
dM/dT
0
200
400
600
800
1000
T [ºC]

Figure 3

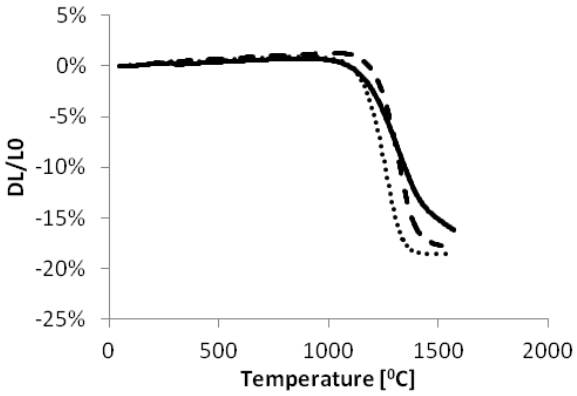

Figure 4.a

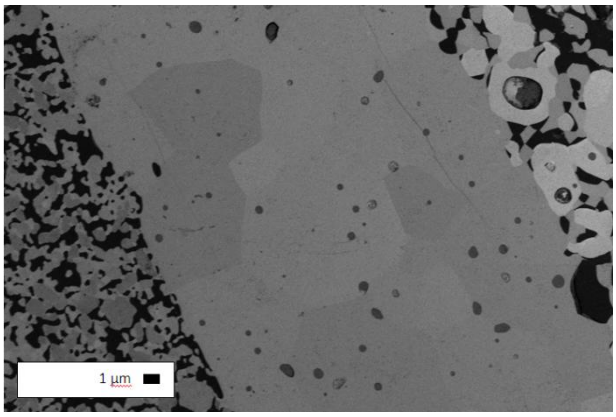

Figure 4.b

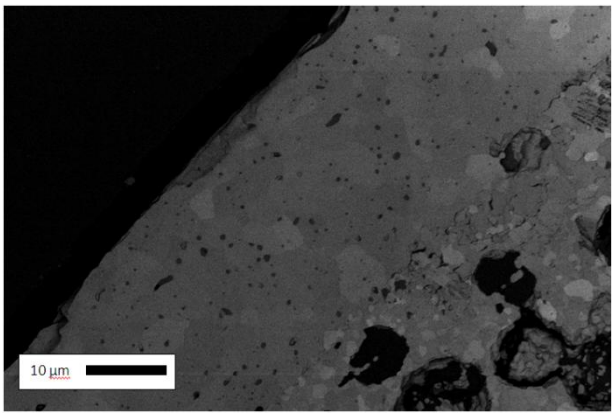

Fig. 5

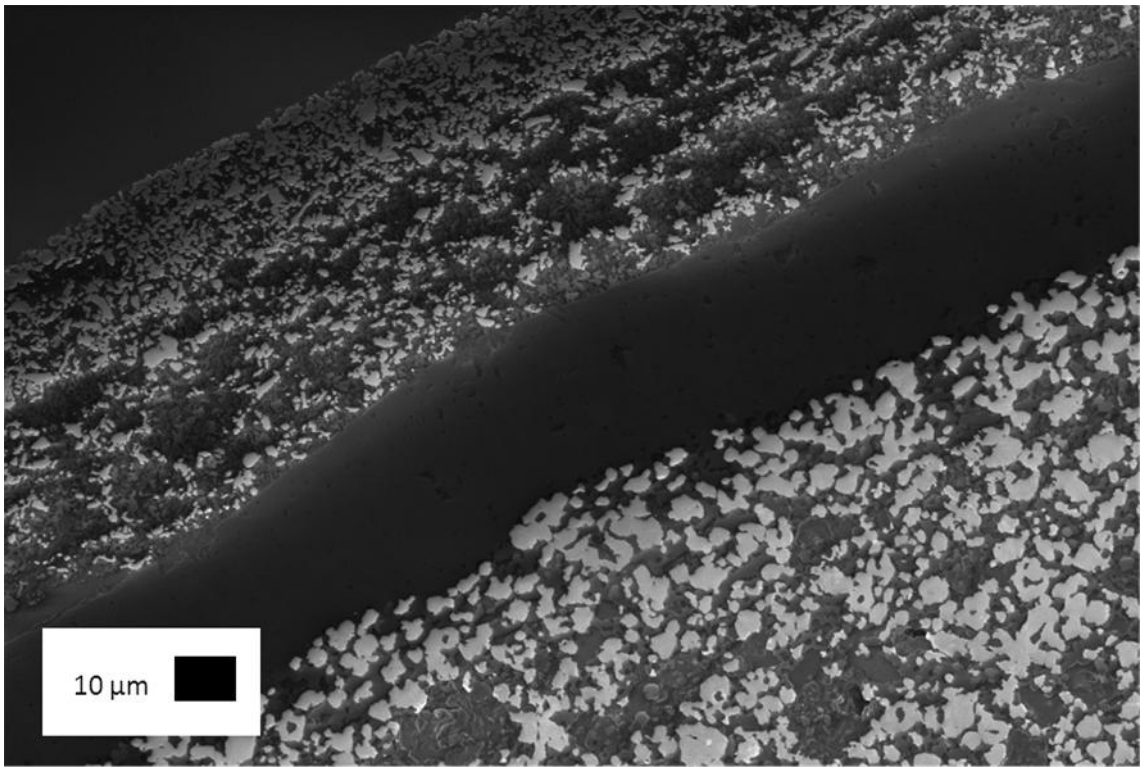

Figure 6.a

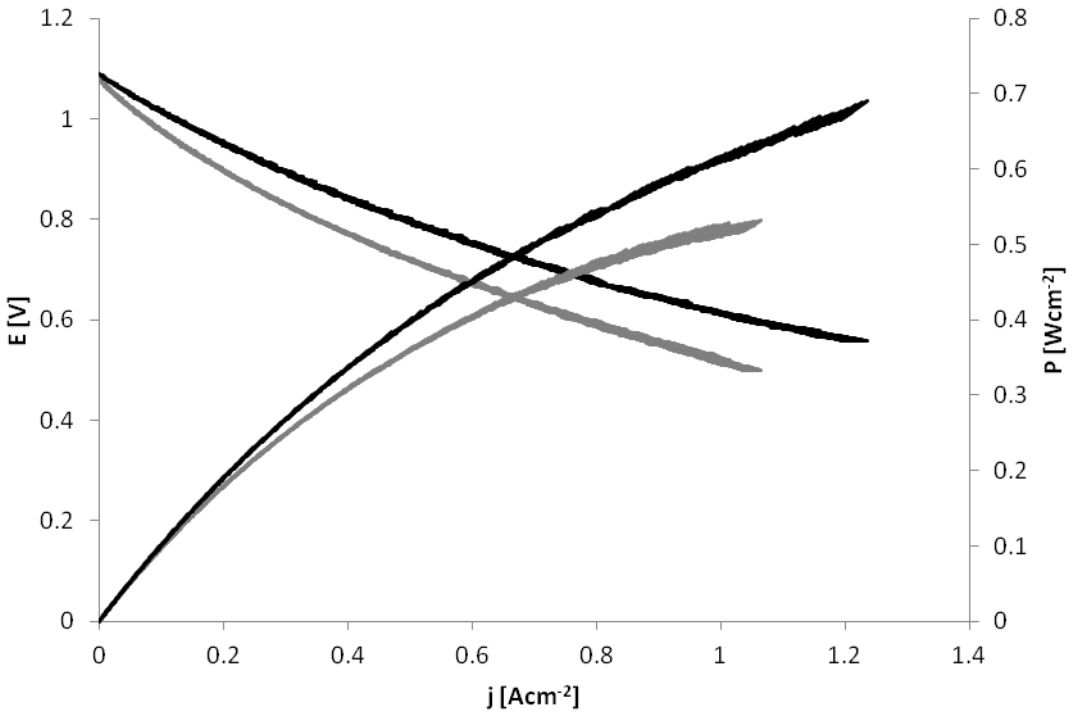
1.2
1
0.8
0.6
0.4
0.2
0
E [V]
0
0.2
0.4
0.6
0.8
1
1.2
1.4
j [Acm-2]
0.8
0.7
0.6
0.5
0.4
0.3
0.2
0.1
0
P [Wcm-2]

Figure 6.b

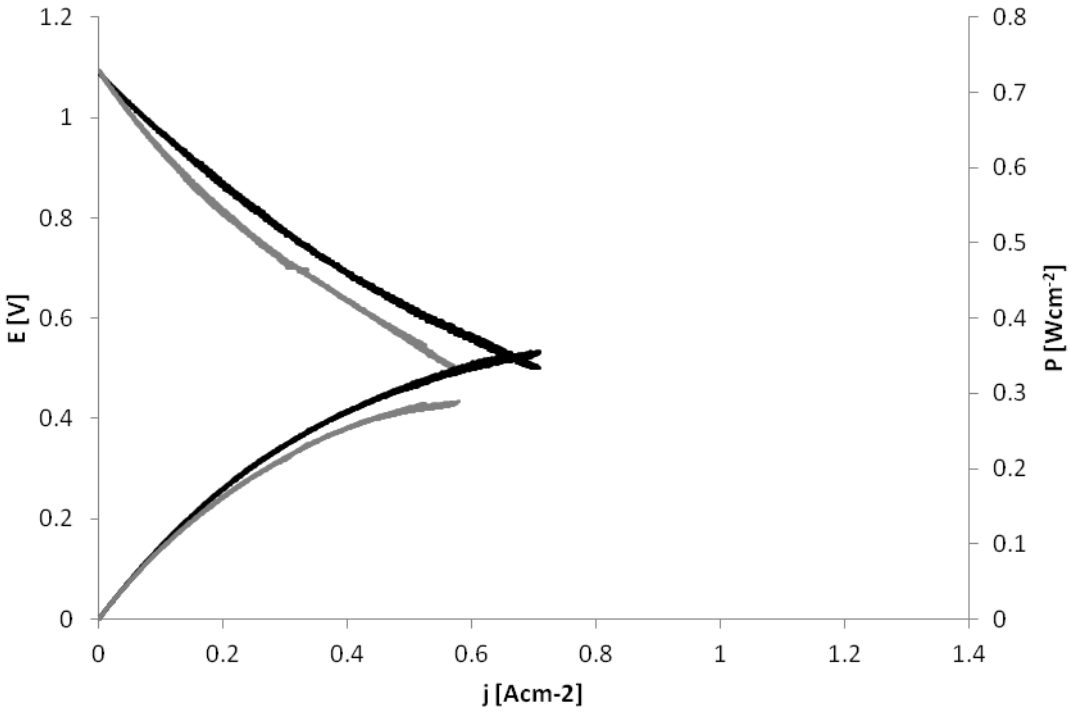
1.2
1
0.8
0.6
0.4
0.2
0
E [V]
0.8
0.7
0.6
0.5
0.4
0.3
0.2
0.1
0
P [Wcm-2]
0
0.2
0.4
0.6
0.8
1
1.2
1.4
j [Acm-2]

Figure 7

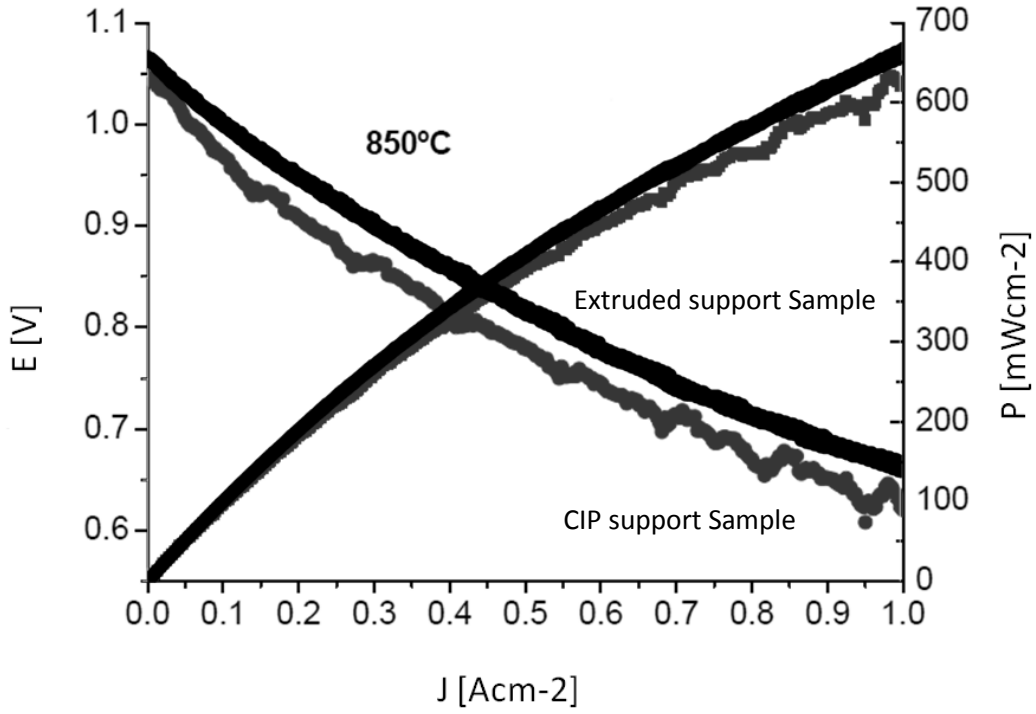
850°C
Extruded support Sample
CIP support Sample
E [V]
P [mWcm-2]
J [Acm-2]
1.1
1.0
0.9
0.8
0.7
0.6
700
600
500
400
300
200
100
0
0.0
0.1
0.2
0.3
0.4
0.5
0.6
0.7
0.8
0.9
1.0

Figure 8.a

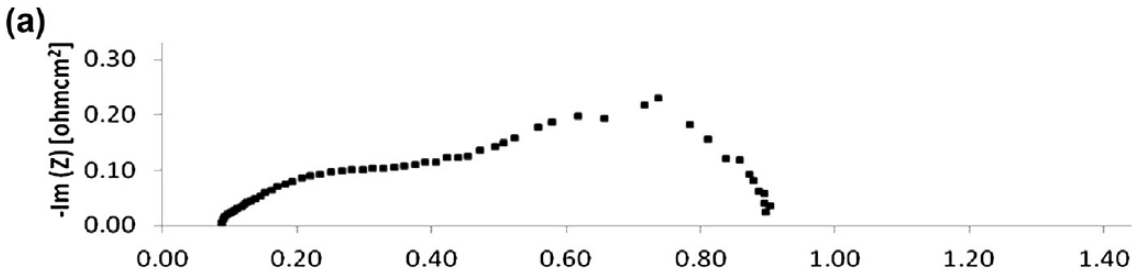

Figure 8.b

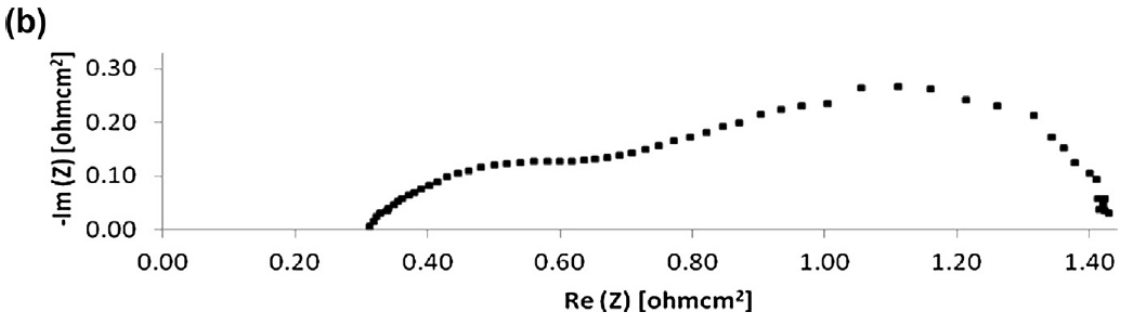
(b)
-Im (Z) [ohmcm²]
0.30
0.20
0.10
0.00
0.00
0.20
0.40
0.60
0.80
1.00
1.20
1.40
Re (Z) [ohmcm²]

References

[1] James Larminie AD. Fuel Cell Systems Explained, 2nd Edition: Wiley; 2003.
[2] Subhash C. Singhal KK. High-temperature Solid Oxide Fuel Cells: Fundamentals, Design, and Applicatons: Elsevier; 2003.
[3] John T.S. Irvine PC. Solid Oxide Fuels Cells: Facts and Figures: Past Present and Future Perspectives for SOFC Technologies: Springer; 2012.
[4] Campana R, Merino RI, Larrea A, Villarreal I, Orera VM. Fabrication, electrochemical characterization and thermal cycling of anode supported microtubular solid oxide fuel cells. J Power Sources. 2009;192:120-5.
[5] Van herle J, Ihringer R, Sammes NM, Tompsett G, Kendall K, Yamada K, et al. Concept and technology of SOFC for electric vehicles. Solid State Ionics. 2000;132:333-42.
[6] Lawlor V. Review of the micro-tubular solid oxide fuel cell (Part II: Cell design issues and research activities). J Power Sources. 2013;240:421-41.
[7] Laguna-Bercero MA, Campana R, Larrea A, Kilner JA, Orera VM. Steam Electrolysis Using a Microtubular Solid Oxide Fuel Cell. J Electrochem Soc. 2010;157:B852-B5.
[8] Laguna-Bercero MA, Campana R, Larrea A, Kilner JA, Orera VM. Performance and Aging of Microtubular YSZ-based Solid Oxide Regenerative Fuel Cells. Fuel Cells. 2010;11:116-23.
[9] Campana R. Pilas de Combustible de Óxido Sólido Microtubulares y Regenerativas en base YSZ o ScSZ de soporte anódico: Universidad de Zaragoza; 2010.
[10] Mahata T, Nair SR, Lenka RK, Sinha PK. Fabrication of Ni-YSZ anode supported tubular SOFC through iso-pressing and co-firing route. Int J Hydrogen Energy. 2012;37:3874-82.
[11] Mirahmadi A, Valefi K. Study of thermal effects on the performance of micro-tubular solid-oxide fuel cells. Ionics. 2011;17:767-83.
[12] Dikwal CM, Bujalski W, Kendall K. The effect of temperature gradients on thermal cycling and isothermal ageing of micro-tubular solid oxide fuel cells. J Power Sources. 2009;193:241-8.
[13] Du Y, Sammes NM. Fabrication and properties of anode-supported tubular solid oxide fuel cells. J Power Sources. 2004;136:66-71.
[14] Lee S-B, Lim T-H, Song R-H, Shin D-R, Dong S-K. Development of a 700W anode-supported micro-tubular SOFC stack for APU applications. Int J Hydrogen Energy. 2008;33:2330-6.
[15] Navarro ME, Capdevila XG, Morales M, Roa JJ, Segarra M. Manufacturing of anode-supported tubular solid oxide fuel cells by a new shaping technique using aqueous gel-casting. J Power Sources. 2012;200:45-52.
[16] Sarkar P, Yamarte L, Rho H, Johanson L. Anode-Supported Tubular Micro-Solid Oxide Fuel Cell. International Journal of Applied Ceramic Technology. 2007;4:103-8.
[17] Othman MHD, Droushiotis N, Wu Z, Kelsall G, Li K. Novel fabrication technique of hollow fibre support for micro-tubular solid oxide fuel cells. J Power Sources. 2011;196:5035-44.
[18] Campana R, Larrea A, Merino RI, Villarreal I, Orera VM. "Mini-Tubular Ysz Based Sofc." Boletin De La Sociedad Espanola De Ceramica Y Vidrio 2008; 47: 189-195.
[19] Monzon H, Laguna-Bercero MA. Redox-cycling studies of anode-supported microtubular solid oxide fuel cells. Int J Hydrogen Energy. 2012;37:7262-70.
[20] Jardiel T, Levenfeld B, Jiménez R, Várez A. Fabrication of 8-YSZ thin-wall tubes by powder extrusion moulding for SOFC electrolytes. Ceram Int. 2009;35:2329-35.
[21] Suzuki T, Yamaguchi T, Fujishiro Y, Awano M. Fabrication and characterization of micro tubular SOFCs for operation in the intermediate temperature. J Power Sources. 2006;160:73-7.
[22] Kim J-D, Kim G-D, Moon J-W, Park Y-i, Lee W-H, Kobayashi K, et al. Characterization of LSM-YSZ composite electrode by ac impedance spectroscopy. Solid State Ionics. 2001;143:379-89.
[23] Jorgensen MJ, Mogensen M. Impedance of Solid Oxide Fuel Cell LSM/YSZ Composite Cathodes. J Electrochem Soc. 2001;148:A433-A42.

[24] Murray EP, Tsai T, Barnett SA. Oxygen transfer processes in (La,Sr)MnO3/Y2O3-stabilized ZrO2 cathodes: an impedance spectroscopy study. Solid State Ionics. 1998;110:235-43.
[25] Gewies S, Bessler WG. Physically Based Impedance Modeling of Ni/YSZ Cermet Anodes. J Electrochem Soc. 2008;155:B937-B52.